Design of a Highly Integrated Electric-Hydraulic Machine for Electrifying Off-Highway Vehicles

FNU Nishanth* *Student Member, IEEE*, Garrett Bohach†, James Van de Ven†, and Eric L. Severson* *Member, IEEE*
*Department of Electrical and Computer Engineering, University of Wisconsin-Madison, Madison, WI 53706 USA
†Department of Mechanical Engineering, University of Minnesota, Minneapolis, MN 55455 USA

***Abstract*—Off-highway vehicles represent a major portion of US energy consumption and greenhouse gas emissions. Electrifying or hybridizing these systems has the potential to yield substantial fuel savings through both efficiency improvements and energy recovery over the drive cycle. However, the extreme power density and transients of these systems pose unique challenges to electrification that have so-far prevented broad commercial success. To overcome these challenges, this paper proposes an integrated electric-to-hydraulic conversion machine. Three novel topologies are proposed which combine the rotor of radial and axial flux machines with an eccentric ball piston hydraulic pump. Design objectives for use in off-highway vehicles are defined, a sizing analysis is performed on each topology, and one topology is selected and optimized to investigate its suitability for meeting the unique requirements of an off-highway vehicle.**

***Index Terms*—Electric-hydraulic conversion, Axial flux motor, Ball piston pump, Multi-objective optimization, Machine design**

I. Introduction

Depleting fossil fuel reserves, growing concern about global warming, and increasingly stringent air quality regulations are spurring interest in the electrification of off-highway vehicles, such as excavators and agriculture equipment. Legacy systems rely on hydraulic power transmission, which suffer from significant throttling and component losses. It is estimated that the average efficiency from the engine shaft to the implement is only 21% [1]. Further, the typical drive cycle of an off-highway vehicle is highly transient in nature, offering substantial opportunities for energy recovery [2]–[5]. Electrification of these systems would enable enormous energy savings by eliminating sources of losses and enabling energy recovery. However, the extreme power density and transient requirements of these vehicles pose unique challenges that cannot be solved by using the electric drivetrain technology developed for passenger vehicles.

Recent research recognizes the need for hybrid hydraulic-electric systems in off-highway vehicles to exploit the benefits of both the hydraulic domain (high power density) and electric domain (elimination of throttle losses, high component efficiency, controllability) [4], [6], [7]. Since the components required to create such a system are all mature technologies (electric machines, hydraulic pumps, variable speed drives), it is tempting to create this system by using off-the-shelf components interfaced together. However, doing this results in a bulky system (low power density) with high inertia (insufficient transient response) and only modest efficiency improvement.

The primary contribution of this paper is to propose a new type of electric-hydraulic conversion machine which integrates the rotor of an electric machine with a hydraulic pump. This approach eliminates redundant bearings, seals, and significantly reduces points of inefficiencies. Furthermore, the hydraulic fluid is easily utilized to cool the electric machine and associated drive electronics, allowing high electric loading. All of this translates to highly desirable benefits of low inertia, high power density, and high electric-hydraulic energy efficiency. The authors have previously investigated a lower power integrated electric-hydraulic conversion machine for a hydraulic charge pump based around a linear motor [8], [9]. The present paper targets a higher power application: the hydraulic actuator of a 20-ton excavator.

In the following sections, key design metrics for off-highway vehicles are presented along with candidate topologies for an integrated electric-hydraulic conversion machine; results from a sizing analysis performed to select the most suitable topology are presented; a preliminary optimization study is conducted on the selected electric machine and the optimal designs are analyzed to determine suitability for the application.

II. Proposed System topologies

The hydraulic actuator of a typical 20-ton excavator is considered as an initial reference application and the corresponding machine design requirements are summarized in Table I. Based on these requirements, this section explores several hydraulic pump and electric machine architectures to determine the most suitable topology for integration.

A. Hydraulic Pump Selection

Selecting a hydraulic pump topology requires knowledge of the operating conditions for the pump unit. In general, the architecture will require four quadrant operation, which necessitates passing through zero speed. Also, it will need to reach maximum speeds of up to 15,000 r/min efficiently. The hydraulic architectures considered were: external gear pump,

This material is based upon work supported by the U.S. Department of Energy Office of Energy Efficiency and Renewable Energy (EERE) under the Award Number DE-EE0008384.
Electromagnetic simulation tools used in this investigation were provided by Mentor Graphics, a Siemens Business.

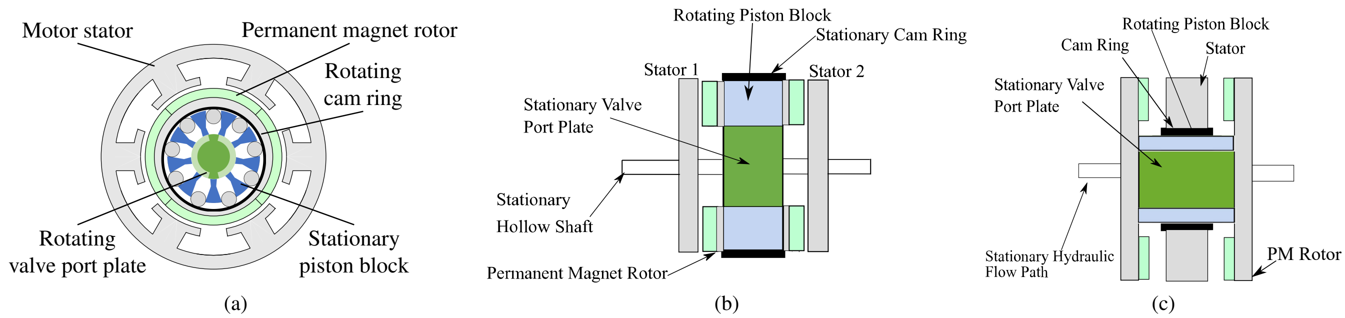

Fig. 1. Proposed system topologies: (a) RF-PMSM based topology; (b) AF-PMSM topology 1; (c) AF-PMSM topology 2.

internal gear pump, gerotor, vane pump, radial piston pump, and axial piston pump.

The ability to integrate the hydraulic architecture into the rotor of the electric machine was paramount, as was the ability to operate in four quadrants. The internal and external gear pumps would need significant modifications to integrate, and the vane architecture has issues with near zero speed operation, which renders it unsuitable. High speeds were a concern for the axial piston architecture because the pistons would start to tip. The radial piston architecture avoids this issue. Further, to increase the power density, a radial ball piston architecture was considered more advantageous than a standard radial piston. Therefore, the radial ball piston and gerotor designs were considered the best architectures for integration, with the radial ball piston eventually being selected. More information on the ball piston pump can be found in [10].

B. Integrated System Topologies

The proposed electric-hydraulic conversion machines are shown in Fig. 1. In all topologies, an eccentric ball piston pump is integrated into the rotor of the electric machine. This pump is shown in detail in Fig. 2 and is used owing to its compact form factor and ability to serve as a bearing interface for the electric machine.

1) RF-PMSM Topology: This topology (Fig. 1a), utilizes a conventional radial flux permanent magnet synchronous machine (RF-PMSM). The hollow PM rotor functions as an eccentric cam ring and the ball piston block is held stationary. Combining the hollow rotor with the piston pump reduces inertia and allows for convenient use of the hydraulic fluid as coolant. However, this topology requires that the pump's valve port plate rotate in order to commutate the hydraulic ports between pistons. This introduces significant mechanical complexity and is viewed as a serious disadvantage.

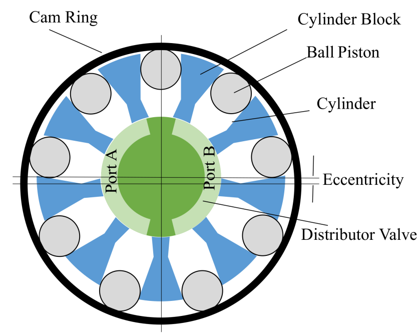

Fig. 2. Eccentric ball piston pump.

2) AF-PMSM Topology 1: In the second topology (Fig. 1b), a two stator axial flux permanent magnet synchronous machine (AF-PMSM) is used. Here, permanent magnets are mounted on either side of the ball piston block, which is now part of the rotor and rotates. A stationary eccentric cam ring causes the pistons to move radially with the rotor's rotation. In this topology, the valve port plate is stationary (an advantage compared to the RF-PMSM topology). However, the design implies that the magnet diameter is equal to the piston block diameter. It will be shown in Section III, that this is not a reasonable constraint for all power and rotational speed combinations.

3) AF-PMSM Topology 2: In this topology, (Fig. 1c), a one stator, dual rotor AF-PMSM is used. In this design, the piston block is again rotated with the magnets, allowing for the use of a stationary valve port plate. However, the magnets are now located radially exterior to the piston block. This allows for the piston block and the magnets to each be designed with a diameter that minimizes their inertia.

TABLE I
DESIGN REQUIREMENTS

Design Objectives	Value
Power	20 kW
Speed	15,000 rpm
Hydraulic flow rate	95.4 L/min
Gravimetric Power Density	5 kW/kg
Cost	<20 $/kW

III. Sizing Analysis of the Proposed Topologies

The specifications for the electric machine and the hydraulic pump are listed in Table II and Table III respectively.

A. Ball Piston Pump Sizing

The ball piston pump's diameter and axial length scale with the design's rated speed and power. This is used to calculate moment of inertia and constrain the dimensions of the electric

TABLE II
ELECTRIC MACHINE SPECIFICATIONS

Parameter	Specification
Rated Rotor Speed (N)	15000 rpm
Power Rating	20 kW
Stator Laminations	M-19 29 Ga
Permanent Magnets	NdFeB
Airgap Flux Density (B_g)	0.8 T
Max. tip speed	150 m/s
Linear Current Density (A_c)	50 A/mm, (rms)

TABLE III
HYDRAULIC PUMP SPECIFICATIONS

Parameter	Specification
Number of pistons (n)	9
High Pressure	14 MPa
Outlet Pressure	2 MPa
Case Pressure	101.3 kPa
Pump Ratio 1 (α)	0.62
Pump Ratio 2 (β)	0.07

machine. Briefly, the diameter of the piston block (D_{pump}) can be calculated as follows

$$D_{\text{pump}} = \frac{1}{\pi}\left(\frac{4nQ}{\beta\alpha^2 N}\right)^{1/3} \tag{1}$$

where n is the number of pistons, Q is the flow rate, N is the rotational speed in revolutions per second. The parameter α is a ratio that relates the ball radius to the circumference, and β is the ratio of eccentricity to the pump diameter. The α and β values used are listed in Table III and were specific to a radial ball piston architecture with nine pistons as described in [11]. The axial length is based off of the piston ball radius r_{ball}

$$r_{\text{ball}} = \frac{\alpha\pi D_{\text{pump}}}{2n} \tag{2}$$

B. Radial Flux Machine Sizing

The radial flux machine is designed using the well known sizing equation as follows

$$T = \frac{\pi}{4} D_o^2 L B_g A_c \tag{3}$$

where D_o is the rotor outer diameter and L is the axial length. The values of B_g and A_c are listed in Table II.

The outer diameter of the rotor (D_o) is constrained by the maximum tip speed (see Table II). The inner diameter available to the pump is determined based on the required magnet thickness and the saturation field level of the rotor back iron. A conservative sizing estimate for the inner diameter is shown in Fig. 3; the advantages of using a higher number of poles are clearly evident at higher speeds.

C. Axial Flux Machine Sizing

Axial flux machines are well-known in the literature, for example [12]–[17], and can typically be designed with a higher power density than radial flux machines. A detailed comparison and derivation of sizing equations is presented

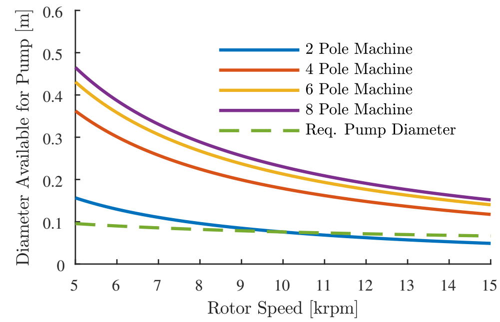

Fig. 3. Maximum available diameter for the piston block in the RF-PMSM topology. The dashed line indicates the required diameter of the pump, as calculated in (1).

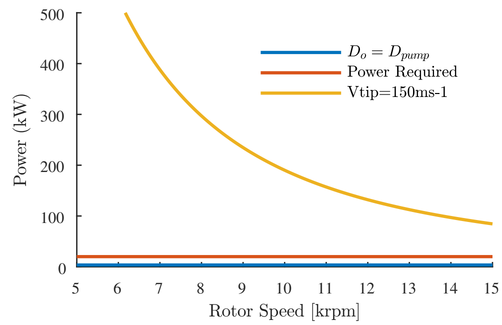

Fig. 4. Power capability of the AF-PMSM; V_{tip} trace corresponds to the rotor tip speed determining the magnet diameter; $D_o = D_{\text{pump}}$ trace corresponds to the magnets having the hydraulic pump diameter.

in [16], [18]. The approach adopted to size the axial flux motor and relate it's geometry parameters to performance is presented in Section IV. It is to be noted that $\lambda = \frac{D_i}{D_o} = 0.63$, ($D_i$ is the inner diameter of the magnets) is used for the preliminary sizing study as this value has been reported in literature to give the best power density for most axial flux motor configurations [16].

Initially, an AF-PMSM of topology 1 (Fig. 1b) is assumed, where the outer diameter of the magnets (D_o) is set to the required diameter of the piston block (D_{pump}) obtained from (1). The resulting machine power is depicted in Fig. 4 and is far below the required 20 kW rating.

Next, the required magnet diameter is calculated to produce the required 20 kW power and shown in Fig. 5a. For AF-PMSM topology 1 to meet the power requirements, the piston block diameter must be increased to match the D_o line, which significantly increases its inertia. Interestingly, Fig. 5a indicates that the magnets are best located exterior to the piston block, which motivates AF-PMSM topology 2.

D. Moment of Inertia Comparison

The moment of inertia for the rotating components of the complete electric-hydraulic machine is calculated for each topology with an 8-pole, 20 kW motor and shown in Fig. 5c. This is a key metric for determining the suitability of each machine topology for application in an off-highway vehicle.

At the 20 kW power level, AF-PMSM topology 2 has a considerable advantage (lower moment of inertia is better). The relative inertia of each component is shown in Fig. 5b, highlighting the wide variations in piston block inertia. In the RF-PMSM, the piston block is stationary and does not contribute to the rotational inertia; however, this topology still is at a significant inertial disadvantage.

E. Flow Ramp Rate Comparison

The hydraulic fluid's flow rate (Q) controls the movement of the hydraulic actuators. Hence, the rate at which the fluid flow rate can be changed, $\frac{dQ}{dt}$, known as the flow ramp rate, determines the speed of response of the system. Therefore, in order to obtain desirable response time, the flow ramp rate is an important parameter. Higher values of flow ramp rate imply a possibility to change the flow rate faster, resulting in quicker response. The machine torque is related to the moment of inertia as $T = J\frac{d\omega}{dt}$; the hydraulic pump flow rate is related to the angular velocity ω and displacement D by the relation $Q = D\omega$. Using these relations, the flow ramp rate and inertia are related as follows

$$\frac{dQ}{dt} = \frac{TD}{J} \tag{4}$$

Using the above relation, the variation of $\frac{dQ}{dt}$ with power rating and rotational speed was plotted in Fig. 6.

It is clear from Fig. 6 that the AF-PMSM topologies offer higher flow ramp rate ($\frac{dQ}{dt}$) at any given power rating and rotor speed. It is also clear that AF-PMSM topology 2 has a much larger $\frac{dQ}{dt}$ at all speeds, making it the topology with the fastest response time.

IV. Axial flux machine modeling and design

A. Axial Flux Motor Design

A detailed discussion on the design of axial flux machines is presented in [16], [18]. A coreless stator design is considered in this paper owing to it's higher efficiency and lower torque ripple [19]. An axial flux motor for the integrated hydraulic-electric conversion machine has a unique set of dimensional constraints imposed by the hydraulic sub-system. This required the conventional design approach to be modified.

The conventional design flow for a double sided axial flux motor makes use of the sizing equation (5) with a certain value of $\lambda = \frac{R_{im}}{R_{om}}$, to obtain the required machine dimensions for a torque/power specified.

$$T = \frac{2\pi}{3} B_g A_c (R_{om}^3 - R_{im}^3) \tag{5}$$

As shown in Fig. 8, the region between R_{om} and R_{im} forms the active conductor length that contributes to torque production. The region between R_{om} and R_{os} as well as the region between R_{is} and R_{im} form the end windings. For maximizing the produced torque, it is therefore preferable to have end-windings outside the active region, which is enforced by setting the conductor width w such that $(R_{os} - R_{om}) = w = (R_{im} - R_{is})$. The axial length of the stator h and the stator inner radius R_{is} are constrained by the hydraulic pump dimensions. Additionally, Table IV summarizes all variables that are explicitly specified in the motor design. Owing to these constraints, the linear current density (A_c) of (5) is calculated as the current density at the machine's inner radius, (R_{im}).

TABLE IV
CONSTANTS FOR ELECTRIC MACHINE DESIGN

Parameter	Symbol	Value
No. of phases	m	3
No. of pole pairs	p	4
No. of stator coils	Q	6
Coil current density	J	10 A/mm^2
Stator inner radius	R_{is}	34 mm
Stator axial length	h	28 mm
Copper packing factor	K_p	0.5

B. 2D Modeling of Axial Flux Machine

The axial flux machine is inherently a 3D-machine. However it has been established in literature that it can be modeled as an equivalent 2D linear machine [20]–[23]. This reduces the computational complexity and greatly speeds up the FEA solves. Hence, a 2D model is more suitable for integrating with an optimization algorithm. Equivalent 2D models can be obtained by introducing radial computation planes as described in [20]. Having a large number of computation planes improves the computation accuracy, but also increases the model evaluation time. The minimum number of computation planes needed to accurately determine the motor parameters from a 2D model depends largely on the motor geometry as described in [21]. It was observed that designs with lower pole-arc to pole-pitch ratio required a large number of computational planes to accurately determine the machine parameters. To prevent these modelling inaccuracies from disrupting the optimization process, the pole arc to pole pitch ratio was fixed to 1 for all designs in this study.

The parameterized 2D-equivalent model is shown in Fig. 9 with equivalent dimensions for the 2D-model calculated as

$$\begin{aligned} w_c &= R_m \frac{2\pi}{Q} \\ w_m &= R_m \frac{2\pi}{2p} \end{aligned} \tag{6}$$

where R_m is the radius at which the computational plane is introduced.

An example design with three computational planes is shown in Fig. 10. The area between R_{im} and R_{om} is subdivided into a number of computation regions based on the accuracy desired. The computation planes are introduced at the average radius of each computation region C_1, C_2, C_3, with the three regions spanning R_{im}–R_2, R_2–R_3, and R_3–R_{om}. The 2D model dimensions for each computation region are obtained by setting R_m equal to the region's computation plane radius (C_1, C_2, or C_3) and evaluating (6).

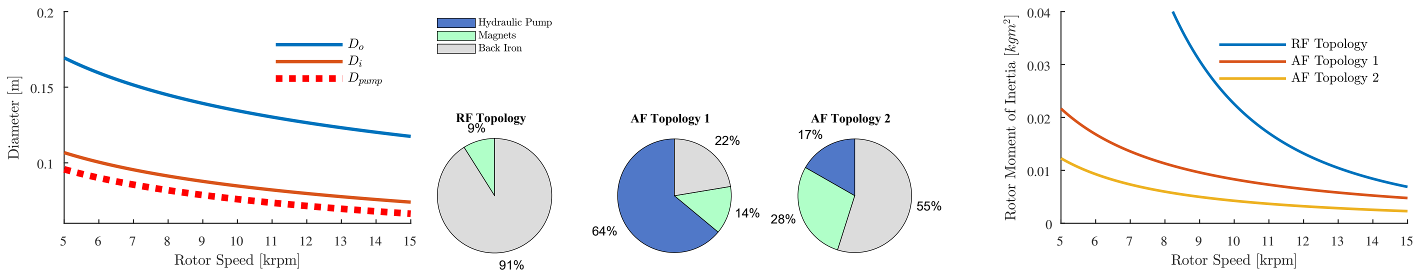

(a) (b) (c)

Fig. 5. Scaling results: (a) Diameter scaling for a 20kW AF-PMSM. D_0 and D_i correspond to the required magnet outer and inner diameters to create the required torque., (b) Contribution of each system component to the total moment of inertia. (c) Moment of inertia of all rotating components of each topology as a function of design rated speed.

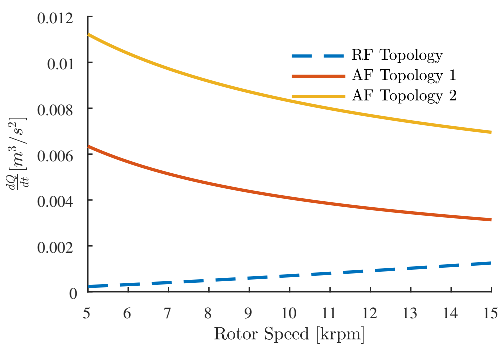

Fig. 6. Flow ramp rate as a function of rated speed.

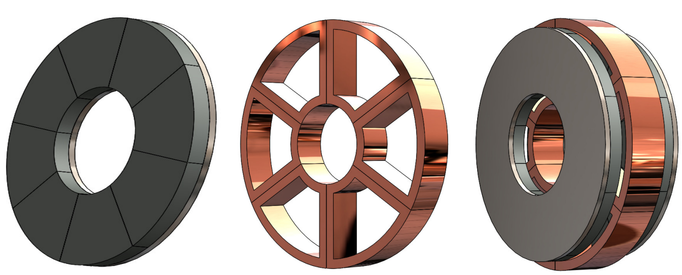

(a) (b) (c)

Fig. 7. 3D view of the selected axial flux machine design: (a) rotor; (b) coreless stator; (c) complete view.

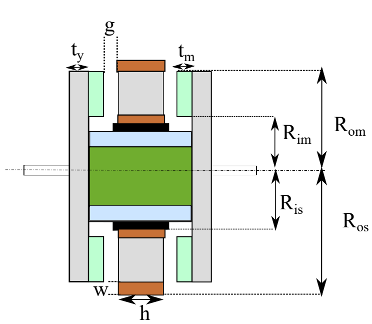

Fig. 8. 2D section view of the axial flux machine.

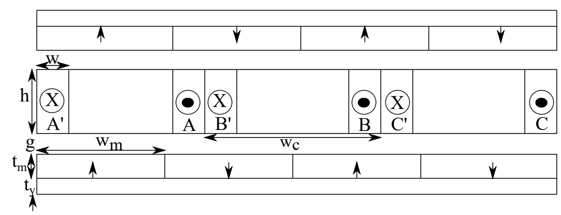

Fig. 9. 2D equivalent model of the AF-PMSM.

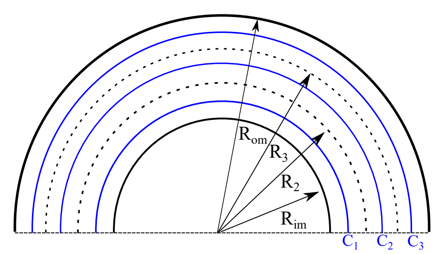

Fig. 10. Computation planes for 2D evaluation.

The motor performance can be estimated from the 2D models as follows: The torque T_i of the computation region corresponding to plane C_i is computed as

$$T_i = \int_{R_{i-1}}^{R_i} \frac{F_x}{R_m} r^2 dr = \frac{F_x}{R_m} \frac{\left(R_i^3 - R_{i-1}^3\right)}{3} \tag{7}$$

where, $R_m = \frac{(R_{i-1}+R_i)}{2}$ and F_x is the force per unit depth obtained from the 2D FEA model. For the example with three computation planes (Fig. 10), torque at plane C_1 can be evaluated by substituting i = 1. R_{i-1} in this case is the magnet inner radius R_{im}. In general, with k computation planes, the net torque can be obtained from the sum

$$T = \sum_{i=1}^{k} T_i \tag{8}$$

A similar approach is adopted to obtain power hysteresis and eddy current losses for the computation region as follows

$$P_i = \int_{R_{i-1}}^{R_i} \frac{P_m}{R_m} r dr = \frac{P_m}{R_m} \frac{\left(R_i^2 - R_{i-1}^2\right)}{2} \tag{9}$$

where P_m is the loss per unit depth of the 2D FEA model evaluated at R_m. The total power loss is obtained by summing the power loss of each computation region obtained from (9).

In order to determine the minimum number of computation planes required to estimate the motor parameters with reasonable accuracy using 2D FEA, 50 random designs were analyzed with computation planes ranging from 1 to 48. The parameters obtained with 48 planes were taken as reference to determine the uncertainty in torque and power; with three computation planes, the uncertainty in torque and power loss determined from 2D model were approximately 1.7% and 3.6% respectively. This was determined to be a reasonable trade-off between accuracy and model evaluation time. Hence, designs were evaluated with three computation planes.

V. Optimization Study

A. Optimization Problem Definition

Considering the unique requirements of off-highway vehicles, the optimization problem is formulated as a multi-objective problem with three objectives: O_1 : Cost [\$/kW], O_2 : Efficiency [%] and O_3 : Torque Ripple [%].

The multi-objective optimization problem can be converted to a single objective optimization by adding suitable weights or can be solved as is, by using a multi-objective algorithm with non-dominated sorting. The non-dominated sort algorithms rely on the concept of Pareto dominance, which can be briefly stated as follows: a candidate design A is said to dominate another candidate design B, if design A is better than design B in at least one objective, and no worse than design B in all of the objectives. Therefore, the non-dominated sort algorithms do not require that weights be attached to any of the objectives, thereby reducing bias and ensuring fairness. In this paper, a multi-objective genetic algorithm (MOGA) with non-dominated sort is used to optimize the electric machine.

B. Variables and Constraints

Table V summarizes the free-variables used in the optimization process and Fig. 9 depicts the geometric parameterization. No constraints are used but designs that fail to produce required torque are scaled analytically as described in Section V-C.

C. Evaluation of Designs

The optimization algorithm is linked to an FEA tool (Mentor Graphics MagNet) which builds and evaluates 2D-equivalent models of the axial flux machine as described in Section IV-B. The torque, iron loss, and loss in the magnets are computed by post-processing the FEA output as described in (7) and (9). The ohmic loss in the stator winding is computed analytically by making use of the current and the resistance of the coils computed based on the geometry parameters.

TABLE V
Variable range for optimization

Variable	Symbol	Range [mm]
Rotor back iron thickness	t_y	[1, 15]
Magnet thickness	t_m	[3, 25]
Stator coil width	w	[4, 20]
Air gap length	g	[0.5, 4]

TABLE VI
Material cost assumed

Material	Cost [\$/inch^3]
Copper	1.20
M19 Steel	0.28
NdFeB PM	11.61

During the optimization run, certain combinations of free variables can lead to designs that do not produce the rated torque. This could be addressed by imposing an optimization constraint on the design candidate's power rating. However, doing so would significantly lengthen the optimization process. In this paper, a scaling approach is employed to scale candidate designs to the proper power rating.

Equation (7) is used to solve for the scaling laws of the machine as developed in (10) and (11), where T_{rated} is the desired torque rating and T_{FEA} is the torque obtained from FEA for the design being scaled. The losses (in particular, hysterisis and eddy current losses) also need to be determined for the scaled designs. An analytical expression to scale power loss is developed in (12) where $P_{\text{loss, FEA}}$ is the power loss obtained from FEA for the design being scaled.

$$R_{om,\text{scaled}}^3 = \left(R_{om}^3 - R_{im}^3\right) \frac{T_{\text{rated}}}{T_{\text{FEA}}} + R_{im}^3 \tag{10}$$

$$T_{\text{scaled}} = \left(\frac{R_{om,\text{scaled}}^3 - R_{im}^3}{R_{om}^3 - R_{im}^3} \right) T_{\text{FEA}} \tag{11}$$

$$P_{\text{loss, scaled}} = \left(\frac{R_{om,\text{scaled}}^2 - R_{im}^2}{R_{om}^2 - R_{im}^2} \right) P_{\text{loss, FEA}} \tag{12}$$

Finally, the objectives for the designs are computed based on the scaled FEA results as follows:

$$\begin{aligned} O_1 &= C_{\text{kW}} = \frac{C_{\text{PM}} + C_{\text{Cu}} + C_{\text{Steel}}}{P_{\text{out}}} \\ O_2 &= -\eta = \frac{-P_{\text{out}}}{P_{\text{out}} + P_{\text{loss}}} \\ O_3 &= T_{\text{ripple}} = \frac{T_{\max} - T_{\min}}{T_{\text{avg}}} \end{aligned} \tag{13}$$

where P_{out} and P_{loss} are the average output power and power loss; C_{kW} is the cost per kW output power of the machine, which is computed using sum of material costs (PM, copper, M-19 steel) based on the material volume used and rates in Table VI; $T_{\max}$, $T_{\min}$, T_{avg} are the maximum, minimum and average of the torque produced over one electrical cycle.

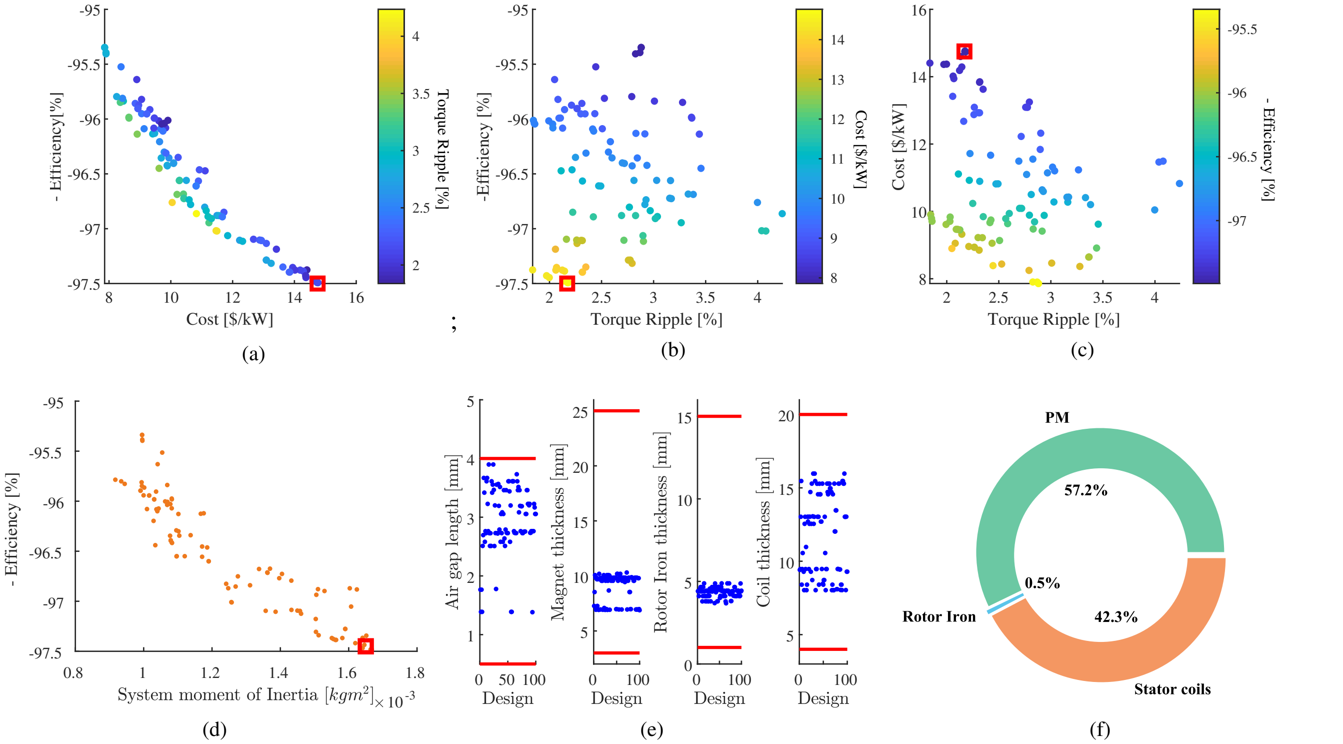

Fig. 11. Optimization results: (a) O_1 versus O_2; (b) O_2 versus O_3; (c) O_3 versus O_1; (d) moment of inertia of the system; (e) variable range; (f) loss break-down for the optimal design.

D. Optimization Results

The optimization was run with 100 individuals for 100 generations, evaluating a total of 10,000 designs. The Pareto front consisting of the candidate designs from the final generation is shown in Fig. 11.

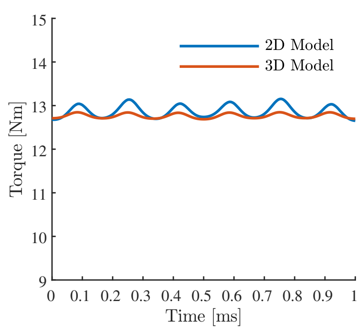

Fig. 12. Torque comparison for an optimal design

It is evident from Fig. 11a that several optimal designs have high efficiency and cost $[\$/kW]$ within the design specification listed in Table I. As the inertia of the system is of paramount importance for the selected application in this paper, moment of inertia is computed for the optimal designs and plotted in Fig. 11d. It can be observed that the optimal designs have moment of inertia in the same range as was theoretically predicted in the sizing study (Fig. 5c) and are indeed suitable for the integrated hydraulic-electric system.

TABLE VII
3D V/S 2D FEA FOR AN OPTIMAL DESIGN

Parameter	3D model	2D model
Average torque [Nm]	12.74	12.89
Stator Ohmic loss [W]	297.80	317.64
Loss in PM [W]	402.58	440.32
Rotor iron loss [W]	3.63	2.44
Torque ripple [%]	1.3	2.43
No. of FEA models	1	3
FEA step size [ms]	0.005	0.005
Total computation time [hrs]	16	0.1

The distribution of free variables within their range, for the optimal designs is shown in Fig. 11e; the candidate designs seem to converge to rotor back iron thickness of about 5 mm and permanent magnet thickness between 7 to 10 mm.

An optimal design was selected from the final generation for detailed analysis. The selected design is indicated in the plots of Fig. 11 by a red box and has the following geometric parameters: $t_m = 9.8$ mm, $t_y = 4.13$ mm, $w = 8.2$ mm, $g = 3.2$ mm, $R_{om} = 97$ mm. CAD renderings of the design are shown in Fig. 7. The design was analyzed using 3D FEA and the results are summarized in Table VII and Fig. 12. Note that the results from 3D and 2D FEA are clearly in close agreement (indicating that the design optimization produced valid results), while the 2D model has a significant reduction in computation time (making the optimization problem feasible to solve).

The selected design clearly meets the design requirements of Table I, while also striking a balance between the competing objectives of high efficiency and low torque ripple. The machine's high reported efficiency (97.5%) does not yet include viscous friction losses associated with the hydraulic fluid within the machine's airgap, nor does it include losses within the pump. The machine's power losses occur predominately within the PM and stator coils (Fig. 11f), both of which are readily cooled by the circulating hydraulic fluid. All of this indicates that this machine is a promising solution for the integrated electic-hydraulic conversion machine application and should be developed further. Additional performance gains and cost reduction are likely possible by varying the magnet pole pitch, allowing the axial flux machine's inner diameter to exceed the pump's outer diameter, or by investigating an iron stator core. The iron stator core is particularly intriguing as a means to reduce the magnet volume, and therefore cost.

Performance improvement in efficiency and inertia is likely to come at the expense of increased torque ripple, which has implications for the broader hydraulic system. Further optimal design will require extending this paper's design framework to accurately model these new design variables, and also quantifying the importance of torque ripple on the hydraulic system. This is beyond the scope of this preliminary investigation, but the authors intend to investigate this in a subsequent publication.

VI. Conclusion and Future Work

This paper presented a novel concept which integrates a hydraulic pump and electric motor into a single machine for electrification of off-highway vehicles. Sizing analysis was used to show that a topology based on a dual rotor axial flux motor with a radial ball piston pump embedded inside of the stator offers the best total system performance potential.

The design problem of the electric machine was formulated to incorporate constraints from the embedded piston pump. The electric machine design was optimized using a proposed 2D FEA modeling technique that incorporates multiple computation regions and design scaling rules. Optimal design candidates are shown to meet the design requirements for electrifying a 20-ton excavator.

Future work on the electric machine design will consider the use of an iron core in the machine's stator to reduce magnet mass and cost. The authors also intend to develop a multiphysics modeling framework to simulate the complete physics of the hydraulic fluid flows coupled with the electromagnetic behavior.

References

[1] L. Love, E. Lanke, and P. Alles, "Estimating the impact (energy, emissions and economics) of the us fluid power industry," *Oak Ridge National Laboratory (ORNL), Oak Ridge, TN*, 2012.

[2] T. Lin, Q. Wang, B. Hu, and W. Gong, "Development of hybrid powered hydraulic construction machinery," *Automation in Construction*, vol. 19, no. 1, pp. 11–19, January 2010.

[3] P. Ponomarev, R. Aman, H. Handroos, P. Immonen, J. Pyrhnen, and L. Laurila, "High power density integrated electro-hydraulic energy converter for heavy hybrid off-highway working vehicles," *IET Electrical Systems in Transportation*, vol. 4, no. 4, pp. 114–121, 2014.

[4] Q. Chen, T. Lin, and H. Ren, "A novel control strategy for an interior permanent magnet synchronous machine of a hybrid hydraulic excavator," *IEEE Access*, vol. 6, 2018.

[5] Z. Du, K. L. Cheong, P. Y. Li, and T. R. Chase, "Fuel economy comparisons of series, parallel and hmt hydraulic hybrid architectures," in *American Control Conference (ACC), 2013*. IEEE, 2013, pp. 5954–5959.

[6] T. A. Minav, J. J. Pyrhonen, and L. I. E. Laurila, "Permanent magnet synchronous machine sizing: Effect on the energy efficiency of an electro-hydraulic forklift," *IEEE Transactions on Industrial Electronics*, vol. 59, no. 6, pp. 2466–2474, June 2012.

[7] S. Hui, Y. Lifu, and J. Junqing, "Hydraulic/electric synergy system (hess) design for heavy hybrid vehicles," *Energy*, vol. 35, no. 12, pp. 5328–5335, 2010.

[8] A. Khamitov, J. Swanson, E. L. Severson, and J. V. de Ven, "Linear electric machine design for an off-highway vehicle hydraulic charge pump," in *2019 IEEE Transportation Electrification Conference and Expo (ITEC)*, June 2019, pp. 1–8.

[9] A. Khamitov, J. Swanson, J. V. de Ven, and E. L. Severson, "Modeling and design of a linear electric-hydraulic conversion machine for electrification of off-highway vehicles," in *2019 Energy Conversion Congress and Exposition (ECCE), IEEE*, September 2019, pp. 1–8.

[10] L. Xu, C. Wei, C. Jing, and J. Liu, "A study on force and lubrication characteristics of ball piston in eccentric ball piston pump," *ASME. Journal of Tribology*, vol. 139, no. 4, April 2017.

[11] G. Bohach, F. Nishanth, E. L. Severson, and J. D. Van de Ven, "Optimization study of a tightly integrated rotary electric motor-hydraulic pump," in *ASME/BATH Symposium on Fluid Power and Motion Control (FPMC), 2019. Sarasota, FL, October 7-9, 2019 (Accepted)*. ASME, 2019.

[12] K. Sitapati and R. Krishnan, "Performance comparisons of radial and axial field, permanent-magnet, brushless machines," *IEEE Transactions on Industry Applications*, vol. 37, no. 5, pp. 1219–1226, Sep. 2001.

[13] A. Chen, R. Nilssen, and A. Nysveen, "Performance comparisons among radial-flux, multistage axial-flux, and three-phase transverse-flux pm machines for downhole applications," *IEEE Transactions on Industry Applications*, vol. 46, no. 2, pp. 779–789, March 2010.

[14] A. Cavagnino, M. Lazzari, F. Profumo, and A. Tenconi, "A comparison between the axial flux and the radial flux structures for pm synchronous motors," *IEEE Transactions on Industry Applications*, vol. 38, no. 6, pp. 1517–1524, Nov 2002.

[15] A. Parviainen, M. Niemela, J. Pyrhonen, and J. Mantere, "Performance comparison between low-speed axial-flux and radial-flux permanent-magnet machines including mechanical constraints," in *IEEE International Conference on Electric Machines and Drives, 2005.*, May 2005, pp. 1695–1702.

[16] S. Huang, J. Luo, F. Leonardi, and T. A. Lipo, "A comparison of power density for axial flux machines based on general purpose sizing equations," *IEEE Transactions on Energy Conversion*, vol. 14, no. 2, pp. 185–192, June 1999.

[17] M. Liben and D. Ludois, "Analytical design of an easily manufacturable, air-cooled, toroidally wound permanent magnet ring motor with integrated propeller for electric rotorcraft," in *2019 IEEE Energy Conversion Congress and Exposition (Accepted)*, 2019.

[18] J. F. Gieras, R.-J. Wang, and M. J. Kamper, *Axial flux permanent magnet brushless machines*. Springer Science & Business Media, 2008.

[19] N. Taran, V. Rallabandi, G. Heins, and D. M. Ionel, "Coreless and conventional axial flux permanent magnet motors for solar cars," *IEEE Transactions on Industry Applications*, vol. 54, no. 6, pp. 5907–5917, Nov 2018.

[20] A. Parviainen, M. Niemela, and J. Pyrhonen, "Modeling of axial flux permanent-magnet machines," *IEEE Transactions on Industry Applications*, vol. 40, no. 5, pp. 1333–1340, 2004.

[21] M. Gulec and M. Aydin, "Implementation of different 2d finite element modelling approaches in axial flux permanent magnet disc machines," *IET Electric Power Applications*, vol. 12, no. 2, pp. 195–202, 2017.

[22] Rong-Jie Wang, M. J. Kamper, K. Van der Westhuizen, and J. F. Gieras, "Optimal design of a coreless stator axial flux permanent-magnet generator," *IEEE Transactions on Magnetics*, vol. 41, no. 1, pp. 55–64, Jan 2005.

[23] V. Rallabandi, N. Taran, D. M. Ionel, and I. G. Boldea, "Magnus an ultra-high specific torque pm axial flux type motor with flux focusing and modulation," in *2017 IEEE Energy Conversion Congress and Exposition (ECCE)*, Oct 2017, pp. 1234–1239.